



Obrabotka metallov -

Metal Working and Material Science


Journal homepage: [http://journals.nstu.ru/obrabotka\\_metallov](http://journals.nstu.ru/obrabotka_metallov)



## Effect of heat treatment on the structure and properties of high-entropy alloy $\text{AlCoCrFeNiNb}_{0.25}$

Zhanna Kovalevskaya <sup>a, \*</sup>, Yuanxun Liu <sup>b</sup>

National Research Tomsk Polytechnic University, 30 Lenin Avenue, Tomsk, 634050, Russian Federation

<sup>a</sup>  <https://orcid.org/0000-0003-3040-8851>,  [kovalevskaya@tpu.ru](mailto:kovalevskaya@tpu.ru); <sup>b</sup>  <https://orcid.org/0009-0002-8501-2643>,  [yuansyunl@tpu.ru](mailto:yuansyunl@tpu.ru)

### ARTICLE INFO

#### Article history:

Received: 10 April 2025

Revised: 24 April 2025

Accepted: 13 June 2025

Available online: 15 September 2025

#### Keywords:

High-Entropy Alloy

$\text{AlCoCrFeNiNb}_{0.25}$

Heat Treatment

Microstructure

Microhardness

Compression Tests

### ABSTRACT

**Introduction.** Currently, one of the most studied high-entropy alloys (*HEAs*) is the *CoCrFeNi* system with the addition of a fifth component. An example of such an alloy is *AlCoCrFeNi* alloyed with additional elements. *Nb* alloying promotes the formation of a solid solution and a secondary *Laves* phase in the alloy, and leads to the formation of eutectics between these phases. The optimal combination of mechanical properties achieved in the hypoeutectic alloy  $\text{AlCoCrFeNiNb}_{0.25}$  was the basis for the choice of this alloy for further studies under heat treatment conditions. **Purpose of the work.** To investigate the effect of heat treatment, including heating to temperatures of 900°C, 1,000°C and 1,100°C with subsequent cooling in air, on the structure and properties of  $\text{AlCoCrFeNiNb}_{0.25}$ . **The methods of investigation** were optical metallography, X-ray diffraction analysis, microhardness measurement, and compression tests. **Results and Discussion.**  $\text{AlCoCrFeNiNb}_{0.25}$  alloy retains the solid solution structure based on the *BCC* phase not only in the cast state, but also after heat treatment. Irrespective of heat treatment parameters, the alloy retains the hypoeutectic structure consisting of solid solution dendrites and eutectic with the *Laves* phase in the interdendritic space. Heat treatment leads to changes in the phase composition of the alloy and refinement of structural components. When heated to 900°C, along with the existing solid solution and *Laves* phase,  $\sigma$ -phase is released in the structure, which increases the microhardness of the alloy, but does not provide improvement of strength properties due to its low plasticity. The strength properties of the alloy are significantly improved by heat treatment with heating up to 1,000°C and 1,100°C. Heating up to 1,100°C is accompanied by an increase in residual strain. The main reasons for this effect may be transformations occurring both in the solid solution of the *BCC* phase (dissolution of the *B<sub>2</sub>* phase, rearrangement of the substructure, increase in the lattice parameter) and in the eutectic (increase in the proportion of the *Laves* phase, refinement of eutectic cells).

**For citation:** Kovalevskaya Z.G., Liu Y. Effect of heat treatment on the structure and properties of high-entropy alloy  $\text{AlCoCrFeNiNb}_{0.25}$ . *Obrabotka metallov (tekhnologiya, oborudovanie, instrumenty)* = *Metal Working and Material Science*, 2025, vol. 27, no. 3, pp. 137–150. DOI: 10.17212/1994-6309-2025-27.3-137-150. (In Russian).

## Introduction

For over two decades, the global community of materials scientists has been developing and investigating a novel class of metal alloys, known as high-entropy alloys (*HEAs*) [1–4]. Unlike conventional metal alloys with a single principal component, *HEAs* are composed of multiple principal components in equiatomic or near-equiatomic concentrations [3]. Due to the high mixing entropy, *HEAs* typically exhibit disordered solid solutions. This phase configuration endows them with enhanced strengthening capabilities and favorable ductility characteristics, making *HEAs* promising candidates for structural materials [4–6]. One of the most extensively studied systems is the *CoCrFeNi* alloy, which is often modified by the addition of a fifth element, such as *Cu*, *Mo*, *Mn*, or *Al* [7–11]. For instance, the thoroughly studied *AlCoCrFeNi* alloy demonstrates excellent synergy of its constituents, as well as the ability to control its phase composition and structure by heat treatment. Consequently, the resulting alloy achieves an advantageous combination of strength and ductility properties [12–19].

In the search for optimal *HEA* compositions for the manufacture of machine components, contemporary researchers are advancing in two primary directions: either reducing/increasing the content of one of the

#### \* Corresponding author

Kovalevskaya Zhanna G., D.Sc. (Engineering), Professor  
National Research Tomsk Polytechnic University,  
30 Lenin ave.,  
634050, Tomsk, Russian Federation  
Tel.: +7 3822 706-351, e-mail: [kovalevskaya@tpu.ru](mailto:kovalevskaya@tpu.ru)

components of the existing *HEAs* [6, 19–21] or introducing additional elements as alloying agents, such as *Ti*, *Zr*, *Si*, *V*, *C*, *Nb*, and others [22–27].

Several studies have demonstrated the effect of *Nb* doping on the structure and properties of *AlCoCrFeNi* and related *HEA* systems [28–31]. It is well established that *Nb* and the *HEA* components exhibit negative mixing enthalpies. Furthermore, *Nb* possesses the largest atomic size in the system. These characteristics of *Nb* contribute to the formation, on one hand, of a stable solid solution with enhanced interatomic bonds, and on the other hand, of secondary phases that are essential for alloy strengthening. For instance, the work [28] showed that *Nb* doping of the *AlCoCrFeNi* *HEA* resulted in the formation of a eutectic structure that included the ordered *Laves* phase (*CoCr*)*Nb*. This leads to alterations in the microstructure and properties of the alloy, where the compressive yield strength and hardness increase, while ductility decreases. An optimal combination of mechanical properties is achieved in the hypoeutectic *AlCoCrFeNiNb*<sub>0.25</sub> alloy, which was chosen for this investigation.

Various heat treatment methods, including annealing and quenching, are employed to strengthen *HEAs* [20, 32–37]. In certain instances, heat treatment can enhance both strength and ductility of *HEAs* [5]. This unique effect, which is not typical for conventional alloys, necessitates thorough investigation and analysis.

The **purpose of this paper** is to investigate the effect of heat treatment on the structure and properties of the *AlCoCrFeNiNb*<sub>0.25</sub> high-entropy alloy (*HEA*). The heat treatment process involves heating to 900 °C, 1,000 °C, and 1,100 °C followed by air cooling.

## Methods

The *AlCoCrFeNiNb*<sub>0.25</sub> alloy with a near-equiatomic composition was produced by the arc melting method in a water-cooled copper crucible under an argon atmosphere. The alloy, whose chemical composition is detailed in Table 1, was made of components with more than 99.5 wt. % purity. To ensure the homogeneity of the chemical composition, the ingot was remelted at least five times. The dimensions of the resulting ingot were 70×35×12 mm. Prior to heat treatment, ingots were cut into fragments measuring 35×12×6 mm. After heat treatment, the central portions of the fragments were further cut into parallelepipeds measuring 10×4×4 mm. The cut samples were polished and used for compression testing. The remaining portions of the fragments were utilized for X-ray diffraction analysis, microstructural evaluation, and microhardness measurements.

Table 1

Chemical composition of *AlCoCrFeNiNb*<sub>0.25</sub> (at.% and wt.%)

Element	<i>Al</i>	<i>Co</i>	<i>Cr</i>	<i>Ni</i>	<i>Fe</i>	<i>Nb</i>
at.%	19.1	19.1	19.1	19.1	19.1	4.5
wt.%	9.8	21.5	18.9	21.4	20.4	8.0

Samples of the *AlCoCrFeNiNb*<sub>0.25</sub> alloy were heat-treated as follows: heating to 900 °C, 1,000 °C, and 1,100 °C, holding for 1 h, and air cooling. For simplicity, the heat-treated samples were designated as *T900*, *T1000*, and *T1100*, respectively while the as-cast sample was designated *T30*.

Thin sections were prepared from the samples, and their microstructure was analyzed using an *Axio Observer Alm* optical microscope and a *Quanta 200* scanning electron microscope (*SEM*) equipped with an *EDAX* energy-dispersive X-ray spectroscopy (*EDS*) unit. The phase composition was determined using an *XRD-6000* diffractometer with *Cu-K $\alpha$*  radiation. The scanning angles ranged from 20° to 80° with a step of 0.02°. Microhardness measurements were performed with a *PMT-3* hardness tester with a load of 100 g. Compression tests were performed using a universal testing machine (*MTS SANS CMT5105*) at a compression rate of 5×10<sup>−3</sup> mm/s. At least three samples per treatment condition were measured.

## Results and Discussion

Fig. 1, *a* shows X-ray diffraction (XRD) patterns of the  $AlCoCrFeNiNb_{0.25}$  alloy in the as-cast state and after heat treatment. In the as-cast state, the alloy consists of a primary *BCC* phase, which represents a disordered solid solution of all components present in the system. The disorder of the solid solution in the primary phase is attributed to the redistribution of components with various atomic radii in the *BCC* lattice and their segregation into two phases with different parameters. The solid solution disorder manifests in the XRD pattern as splitting of the main *BCC* peak into two distinct peaks (Fig. 1, *b*). Furthermore, the XRD pattern exhibits peaks corresponding to the crystal lattice of the *Nb*-rich *Laves* phase, which can be identified as  $(CoCr)Nb$  with a hexagonal structure, as well as the [001] reflection peak of the *B2* phase representing  $AlNi$  with a *BCC* lattice [29, 32].

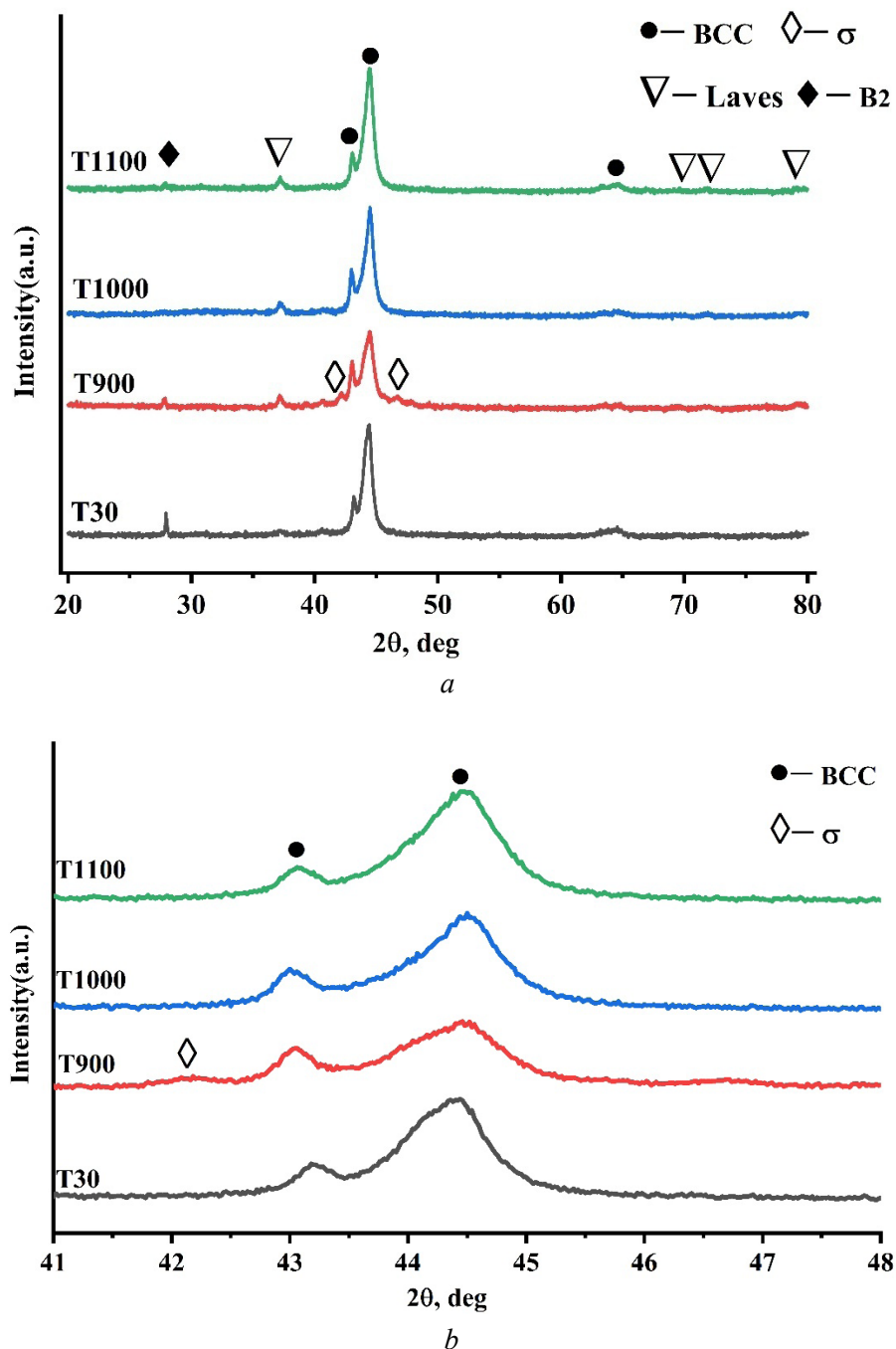


Fig. 1. XRD patterns of  $AlCoCrFeNiNb_{0.25}$  alloy in the as-cast state and after heat treatment (*a*) with enlarged image in the  $2\theta$  range of  $41-48^\circ$  (*b*)

The existence of the *Laves* phase is characteristic of *AlFeNiCoCrNb* alloys where the *Nb* concentration corresponds to a molar ratio of 0.25 or higher. In this case, *Nb* not only dissolves in the primary *BCC* phase but also promotes the formation of the secondary – *Laves* – phase, which forms a eutectic mixture with the *BCC* phase [29].

According to the findings of [32], during cooling of the *AlFeNiCoCr* alloy, the primary crystallized *BCC* phase may incoherently separate into a mixture of an unordered *BCC* phase enriched in *Cr-Fe* and an ordered *B2* phase enriched in *Al-Ni*, which is evidenced by the presence of a peak corresponding to the *B2* phase in the *XRD* pattern.

Subsequent heat treatment of the alloy leads to the following changes in the *XRD* patterns. As the heating temperature increases, the intensity of the *B2*-phase peak decreases, while the intensity of the peak corresponding to the *Laves* phase slightly increases. In addition, changes occur in the lattice of the primary *BCC* phase. Fig. 1, *b* presents an enlarged view of the (110) peak of the *BCC* phase. It is evident that, with an increase in the heating temperature, the peak shifts towards smaller angles, indicating an increase in the lattice parameter of the *BCC* solid solution, which suggests changes in the composition of the solid solution.

After heat treatment at 900 °C, peaks of a new phase emerge, which is identified as the tetragonal  $\sigma$  phase composed of *Cr* and *Fe*. The  $\sigma$  phase is absent at higher heating temperatures. The phenomenon of the  $\sigma$ -phase precipitation and dissolution in the *BCC* phase within a similar temperature range was also observed previously [29].

The *XRD* analysis of the *AlCoCrFeNiNb*<sub>0.25</sub> alloy throughout the entire heating temperature range shows that the primary phase remains an unordered *BCC* solid solution. However, upon heating of the *AlFeNiCoCr* alloy without *Nb*, part of the material transforms into an *FCC* solid solution [29]. Thus, the addition of *Nb* helps stabilize the *BCC* phase and maintain a predominantly single-phase structure in the high-entropy alloy.

Fig. 2 depicts the microstructure of the *AlCoCrFeNiNb*<sub>0.25</sub> alloy both in the as-cast state and after heat treatment. The alloy consistently exhibits a dendritic morphology with hypoeutectic characteristics. The microstructure comprises primary dendritic and interdendritic eutectic regions. Dendritic regions consist of a *BCC* phase, while the eutectic structure is a mixture of the *BCC* and *Laves* phases. In the as-cast state, dendritic segregation results in compositional heterogeneity: dendritic cores (*BCC* phase) are enriched in *Ni* and *Al*, whereas the dendritic periphery and eutectic regions are enriched in *Cr* and *Fe*. *Nb* partially dissolves in the *BCC* phase, but most of it enters the composition of the *Laves* phase [29]. Results of the elemental analysis in different zones of the as-cast alloy are detailed in Table 2. The same pattern of formation of the dendritic structure in the alloy was reported in [15, 29].

The dendritic structure that exhibits a dark contrast after etching is surrounded by lighter layers of the *Laves* phase, which represents a secondary phase. The secondary *Laves* phase forms along the solid solution boundaries during dendritic growth and is attributed to the reduced solubility of niobium in the solid solution of the principal components during cooling. The enrichment of the peripheral regions of dendrites with niobium and chromium creates conditions for the formation of the secondary *Laves* phase based on these components.

Fig. 2, *b* shows a defective eutectic structure. Grains of the *Laves* phase are divided into fragments with random crystallographic orientations. Since the eutectic, which includes the *Laves* phase, forms in the interdendritic space, it is structurally impossible to distinguish between the secondary *Laves* phase and the *Laves* phase present in the eutectic.

Heat treatment at 900–1,100 °C does not alter the dendritic structure of the alloy (Fig. 2). The dendrite width along the secondary axes ranges from 11 to 15  $\mu\text{m}$ . Increasing the heating temperature from 900 °C to 1,100 °C leads to changes in the structure of the eutectic, this can be observed in high-magnification metallographic images (Figs. 2, *f*, *h*). At the heating temperature of 900 °C, no noticeable changes in the eutectic structure occur. However, at 1,000 °C, *Laves* phase fragments begin to align, which is typical of the eutectic, and the formed lines alternate with the solid solution. At 1,100 °C, eutectic grains are well defined in the interdendritic space (Fig. 2, *h*). The *XRD* analysis confirms the eutectic transformation: the peak intensity of the *Laves* phase increases with temperature. This may arise from either the coalescence of



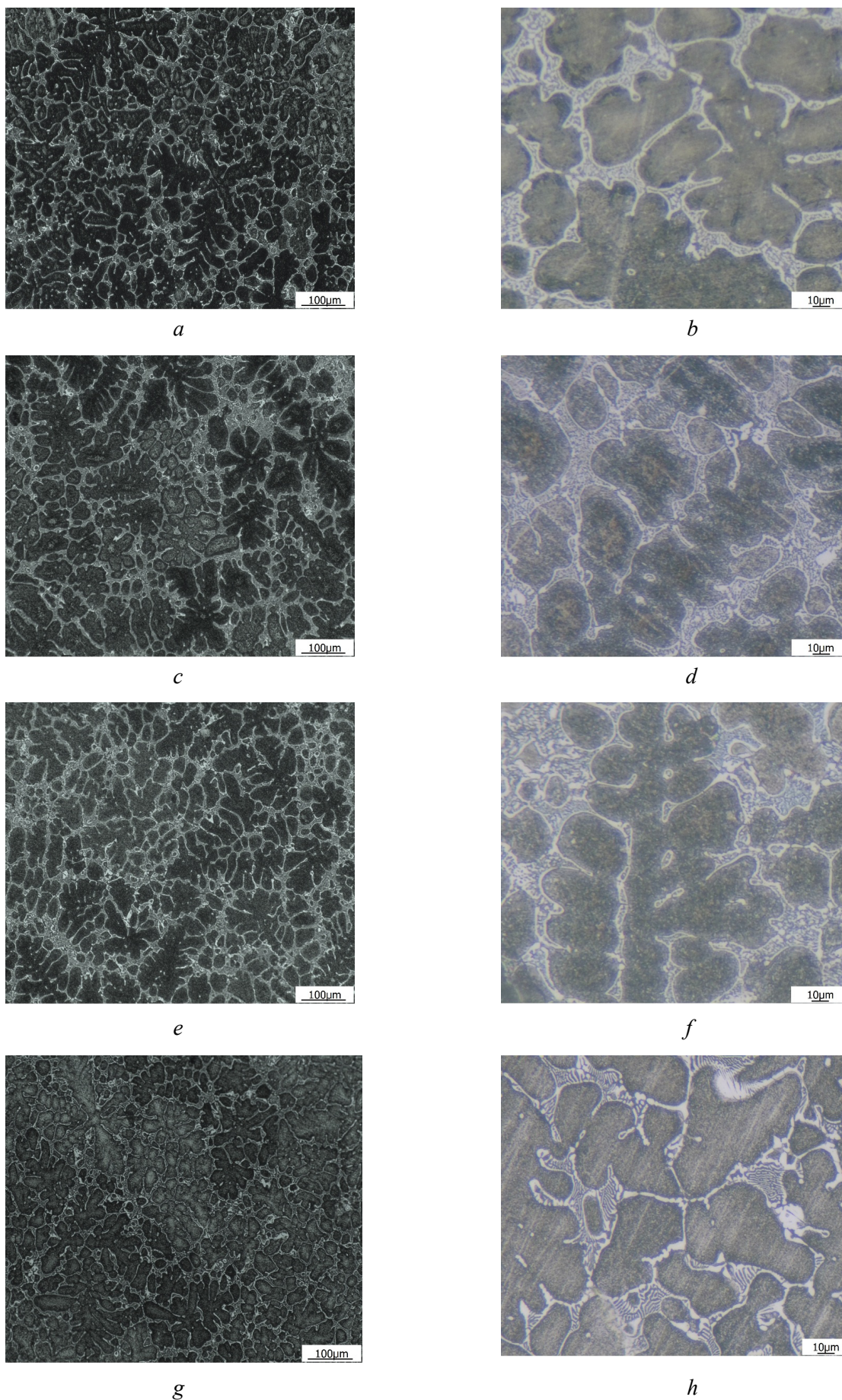


Fig. 2. Microstructure of  $AlCoCrFeNiNb_{0.25}$  alloy in the as-cast state and after heat treatment: T30 (a, b); T900 (c, d); T1000 (e, f); T1100 (g, h)

Table 2

Chemical compositions (at.%) in the *AlCoCrFeNi* alloy in the as-cast state

<i>T30</i>	<i>Al</i>	<i>Cr</i>	<i>Fe</i>	<i>Co</i>	<i>Ni</i>	<i>Nb</i>
Dendrite core	17.76	16.46	18.61	20.30	24.56	2.40
Dendrite periphery	14.85	21.61	20.75	20.14	21.06	1.59
Solid solution in eutectics	12.09	23.86	22.05	19.78	19.28	2.96
<i>Laves</i> phase	3.80	18.36	21.43	23.66	11.56	21.17

secondary-phase grains or from its increased fraction in interdendritic zones via solid solution precipitation (Fig. 1, *a*).

The *XRD* analysis confirms that an ordered  $\sigma$  phase forms in the alloy at 900°C. In [32], it was reported that the  $\sigma$  phase precipitated from the disordered solid solution where it was enriched in *Cr* and *Fe* in the form of dispersed particles. Our *SEM* studies reveal that  $\sigma$ -phase particles are distributed throughout the dendrite volume (Fig. 3, *b*). After heat treatment at 1,000 °C,  $\sigma$ -phase particles are still observed, but in smaller amounts (Fig. 3, *c*). At 1,100 °C, they completely disappear (Fig. 3, *d*).

The *SEM* analysis reveals that heat treatment significantly alters the structure of the solid solution within dendrites (Fig. 3). During alloy solidification, the cooling process leads to the spinodal decomposition of the disordered solid solution into a *Fe*- and *Cr*-enriched disordered solid solution and an ordered *B2* phase enriched in *Ni* and *Al* [32]. This decomposition results in the formation of the so-called basket weave

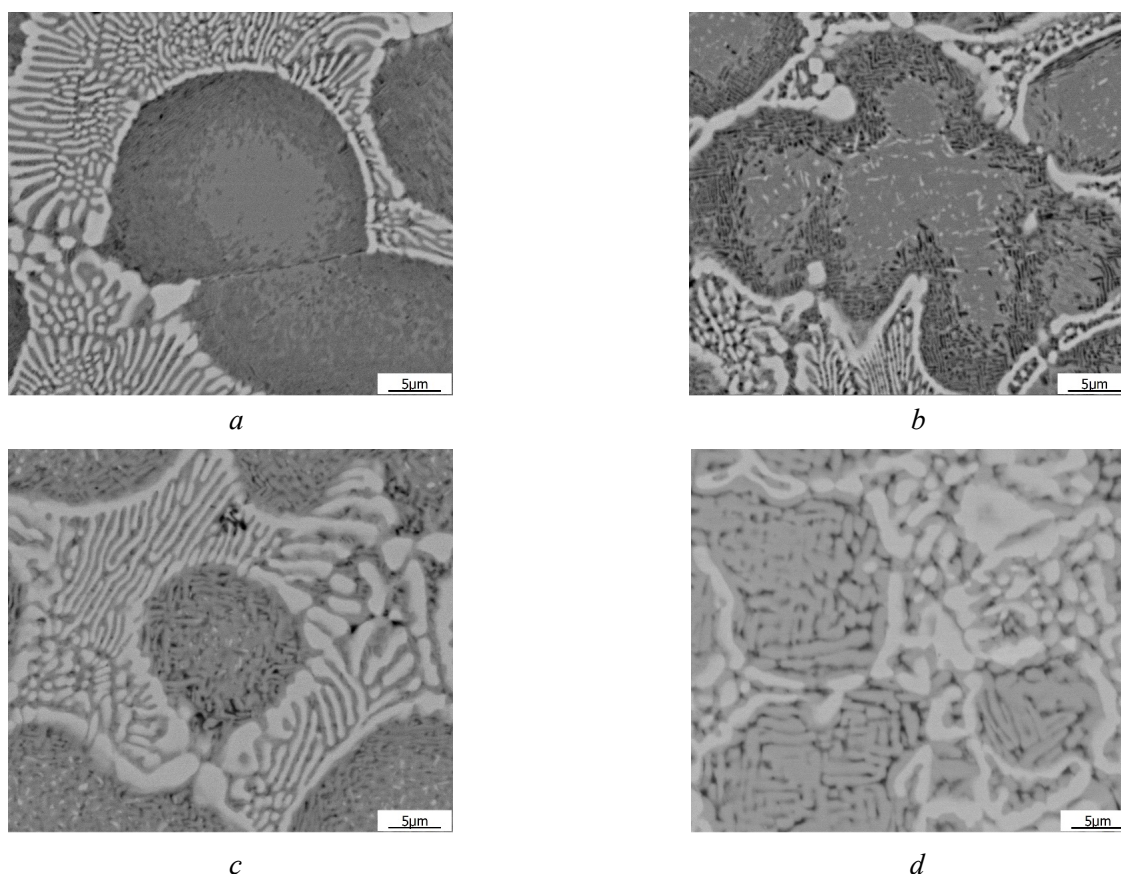


Fig. 3. Microstructure of *AlFeNiCoCrNb*<sub>0.25</sub> alloy in the as-cast state and after heat treatment, obtained using *SEM*: *T30* (*a*); *T900* (*b*); *T1000* (*c*); *T1100* (*d*)



structure, which was described in detail in [15, 32, 37]. In the investigated as-cast alloy, a characteristic basket weave or banded structure forms in the peripheral regions of dendrites, which is attributed to the spinodal decomposition of the solid solution. No banded structure is observed in the center of dendrites (Fig. 3, *a*).

When the alloy is heated to 900 °C and subsequently cooled, structural heterogeneity in dendrites and the basket weave structure become more pronounced (Fig. 3, *b*). Furthermore, as mentioned above,  $\sigma$ -phase particles precipitate from the solid solution. According to X-ray structural analysis, after heat treatment, the proportion of the ordered *B2* phase decreases, suggesting that the observed contrast within the basket weave structure is due not to the spinodal decomposition of the solid solution into two phases but rather to the heterogeneous segregation of atomic components within the disordered solid solution, as described in [15]. At 1,000 °C, the basket weave structure increases in size and occupies the entire volume of dendrites (Fig. 3, *c*). Further heating to 1,100 °C causes coarsening (Fig. 3, *d*).

The average microhardness and the microhardness of the structural components of the alloy are presented in Table 3. In all heat treatment conditions, the interdendritic regions demonstrate significantly higher microhardness compared to the dendritic cores.

Table 3

**Microhardness of  $\text{AlCoCrFeNiNb}_{0.25}$  alloy in the as-cast state and after heat treatment**

Measurement area	<i>T</i> 30 HV	<i>T</i> 900 HV	<i>T</i> 1000 HV	<i>T</i> 1100 HV
Dendrites	614 ± 44	582 ± 37	489 ± 53	520 ± 35
Eutectic	640 ± 47	902 ± 66	620 ± 45	636 ± 46
Average value	625 ± 28	730 ± 47	545 ± 52	572 ± 56

The maximum microhardness in dendrites of the as-cast alloy is attributed to the unique structure of the solid solution of the alloy components, which forms during crystallization and cooling. The spinodal decomposition of the disordered solid solution coupled with the precipitation of the ordered *B2* phase strengthens the alloy. However, heating of the alloy during heat treatment leads to a partial loss of the order characteristic of the *B2* phase, resulting in a decrease in the microhardness of dendrites. Nevertheless, the precipitation of  $\sigma$ -phase particles upon heating to 900 °C allows the microhardness to remain at a high level. When the heating temperature increases to 1,000 °C, the strengthening effect of the  $\sigma$ -phase particles disappears. During heat treatment at 1,100 °C, coalescence of the basket weave structure occurs, leading to the formation of more distinct phase boundaries, possibly due to the increased heterogeneous segregation of atomic components within the solid solution. This, in turn, slightly increases the microhardness in the dendritic zones of the alloy.

In the interdendritic space of the as-cast alloy, the microhardness of the eutectic is only slightly higher than that of the solid solution in dendrites. This means that strengthening due to spinodal decomposition is comparable in magnitude to that due to the *Laves* phase (a solid intermetallic compound) in the eutectic. During heating at 900 °C, as mentioned above,  $\sigma$ -phase particles precipitate from the solid solution and concentrate in the *Cr*-rich interdendritic space. This significantly increases the microhardness of the eutectic due to strengthening of the solid solution with  $\sigma$ -phase particles in its composition. Dispersed  $\sigma$ -phase particles precipitate in the solid solution of all structural components, significantly enhancing the microhardness in dendrites. Heating to 1,000 °C and 1,100 °C leads to the dissolution of  $\sigma$ -phase particles in the primary phase [11], which contributes to a decrease in the microhardness in the interdendritic space to the values of the initial structure. This is due to the removal of the effect of strengthening due to  $\sigma$ -phase particles.

When evaluating the integral microhardness of all structural components of the alloy, the overall trend in the variation of microhardness with heating temperature is retained (Table 3).

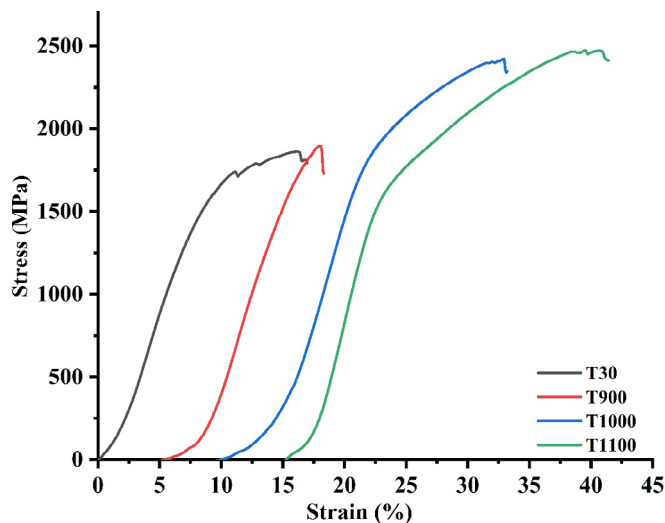


Fig. 4. Compressive stress-strain curves of the  $AlFeNiCoCrNb_{0.25}$  alloy in the as-cast state and after heat treatment

Fig. 4 illustrates compressive stress-strain responses of the as-cast and heat-treated alloys. The offset yield strength, compressive strength, and residual strain are presented in Table 4. The as-cast alloy exhibits good strength and plasticity characteristics. Structural transformations in the alloy during heating to 900 °C have little effect on the strength properties of the material but significantly reduce its plasticity. This reduction is attributed to the precipitation of the brittle  $\sigma$  phase in the structure. The authors of [32] also pointed out the effect of decreased plasticity within a similar temperature range of heat treatment.

During heat treatment at 1,000 °C and 1,100 °C, a significant increase is observed in the strength characteristics of the alloy. At 1,100 °C, the residual strain also increases. Based on the results of XRD analysis and optical microscopy, it

can be suggested that the main reason for this effect is transformations occurring both in the solid solution of the BCC phase ( $B2$ -phase dissolution, substructure rearrangement, and an increase in the lattice parameter) and in the eutectic (increase in the proportion of the *Laves* phase and refinement of eutectic cells). The simultaneous increase in plasticity is likely due to the relief of internal stresses, a reduction in the number of crystalline defects, and coalescence of structural components in dendrites and the eutectic. However, a more precise analysis of this unique effect on the properties of the  $AlCoCrFeNiNb_{0.25}$  alloy requires further research.

Table 4

Offset yield strength, compressive strength and residual strain of  $AlCoCrFeNiNb_{0.25}$  alloy in the as-cast state and after heat treatment

	$\sigma_{0.2}$ (MPa)	$\sigma_u$ (MPa)	$\varepsilon$ (%)
<i>T30</i>	1356	1962	7.7
<i>T900</i>	1605	1894	2.8
<i>T1000</i>	1502	2438	9.8
<i>T1100</i>	1369	2494	16.4

## Conclusions

Doping of the  $AlCoCrFeNi$  high entropy alloy with niobium in a molar ratio of 0.25 led to the stabilization of the solid solution based on the body-centered cubic (BCC) phase both in the as-cast state and after heat treatment involving heating to 900 °C, 1,000 °C, and 1,100 °C followed by air cooling. The resulting structure of the alloy, regardless of the heat treatment modes, consisted of dendrites of the solid solution and a eutectic with the *Laves* phase in the interdendritic space.

Heat treatment altered the phase composition of the alloy and improved its structural components. Upon heating to 900 °C, alongside the already formed solid solution and *Laves* phase, the  $\sigma$  phase precipitated in the structure, which increased the microhardness of the alloy. However, this did not improve the strength properties due to the low plastic characteristics of the  $\sigma$  phase.

The strength characteristics of the alloy significantly increased during heat treatment at 1,000 °C and 1,100 °C. At 1,100 °C, the residual strain also rose. The main reasons for this effect may include





transformations both in the solid solution of the *BCC* phase (such as the *B2*-phase dissolution, substructure rearrangement, and an increase in the lattice parameter) and in the eutectic (an increase in the proportion of the *Laves* phase and refinement of eutectic cells).

### References

1. Yeh J.W., Chen S.K., Lin S.J., Gan J.Y., Chin T.S., Shun T.T., Tsau C.H., Chang S.Y. Nanostructured high-entropy alloys with multiple principal elements: novel alloy design concepts and outcomes. *Advanced Engineering Materials*, 2004, vol. 6, pp. 299–303. DOI: 10.1002/adem.200300567.
2. Cantor B., Chang I.T.H., Knight P., Vincent A.J.B. Microstructural development in equiatomic multicomponent alloys. *Materials Science and Engineering: A*, 2004, vol. 375–377, pp. 213–218. DOI: 10.1016/j.msea.2003.10.257.
3. Gromov V.E., Shlyarova Yu.A., Konovalov S.V., Vorob'ev S.V., Peregudov O.A. Application of high-entropy alloys. *Izvestiya vuzov. Chernaya metallurgiya = Izvestiya. Ferrous Metallurgy*, 2021, vol. 64 (10), pp. 747–754. DOI: 10.17073/0368-0797-2021-10-747-754. (In Russian).
4. Bataeva Z.B., Ruktuev A.A., Ivanov I.V., Yurgin A.B., Bataev I.A. Review of alloys developed using the entropy approach. *Obrabotka metallov (tekhnologiya, oborudovanie, instrumenty) = Metal Working and Material Science*, 2021, vol. 23, no. 2, pp. 116–146. DOI: 10.17212/1994-6309-2021-23.2-116-146. (In Russian).
5. Li W., Xie D., Li D., Zhang Y., Gao Y., Liaw P.K. Mechanical behavior of high-entropy alloys. *Progress in Materials Science*, 2021, vol. 118, p. 100777. DOI: 10.1016/j.pmatsci.2021.100777.
6. Shang Y., Brechtel J., Pistidda C., Liaw P.K. Mechanical behavior of high-entropy alloys: A review. *High-Entropy Materials: Theory, Experiments, and Applications*. Springer, 2021, pp. 435–522. DOI: 10.1007/978-3-030-77641-1\_10.
7. Sheng H.F., Gong M., Peng L.M. Microstructural characterization and mechanical properties of an  $\text{Al}_{0.5}\text{CoCrFeCuNi}$  high-entropy alloy in as-cast and heat-treated/quenched conditions. *Materials Science and Engineering: A*, 2013, vol. 567, pp. 14–20. DOI: 10.1016/j.msea.2013.01.006.
8. Sui Q., Wang Z., Wang J., Xu S., Liu B., Yuan Q., Zhao F., Gong L., Liu J. Additive manufacturing of  $\text{CoCrFeNiMo}$  eutectic high entropy alloy: Microstructure and mechanical properties. *Journal of Alloys and Compounds*, 2022, vol. 913, p. 165239. DOI: 10.1016/j.jallcom.2022.165239.
9. Ruktuev A.A., Lazurenko D.V., Ogneva T.S., Kuzmin R.I., Golkovski M.G., Bataev I.A. Structure and oxidation behavior of  $\text{CoCrFeNiX}$  (where X is Al, Cu, or Mn) coatings obtained by electron beam cladding in air atmosphere. *Surface and Coatings Technology*, 2022, vol. 448, p. 128921. DOI: 10.1016/j.surfcoat.2022.128921.
10. Laplanche G., Kostka A., Horst O.M., Eggeler G., George E.P. Microstructure evolution and critical stress for twinning in the  $\text{CrMnFeCoNi}$  high-entropy alloy. *Acta Materialia*, 2016, vol. 118, pp. 152–163. DOI: 10.1016/j.actamat.2016.07.038.
11. Wang W.R., Wang W.L., Wang S.C., Tsai Y.C., Lai C.H., Yeh J.W. Effects of Al addition on the microstructure and mechanical property of  $\text{AlxCoCrFeNi}$  high-entropy alloys. *Intermetallics*, 2012, vol. 26, pp. 44–51. DOI: 10.1016/j.intermet.2012.03.005.
12. Arun S., Radhika N., Saleh B. Effect of additional alloying elements on microstructure and properties of  $\text{AlCoCrFeNi}$  high entropy alloy system: A comprehensive review. *Metals and Materials International*, 2025, vol. 31 (2), pp. 285–324. DOI: 10.1007/s12540-024-01752-3.
13. Zhang S., Wu C.L., Zhang C.H., Guan M., Tan J.Z. Laser surface alloying of  $\text{FeCoCrAlNi}$  high-entropy alloy on 304 stainless steel to enhance corrosion and cavitation erosion resistance. *Optics & Laser Technology*, 2016, vol. 84, pp. 23–31. DOI: 10.1016/j.optlastec.2016.04.011.
14. Manzoni A., Daoud H., Völkl R., Glatzel U., Wanderka N. Phase separation in equiatomic  $\text{AlCoCrFeNi}$  high-entropy alloy. *Ultramicroscopy*, 2013, vol. 132, pp. 212–215. DOI: 10.1016/j.ultramic.2012.12.015.
15. Wang Y.P., Li B.S., Ren M.X., Yang C., Fu H.Z. Microstructure and compressive properties of  $\text{AlCrFeCoNi}$  high entropy alloy. *Materials Science and Engineering: A*, 2008, vol. 491 (1–2), pp. 154–158. DOI: 10.1016/j.msea.2008.01.064.
16. Kunc I., Polanski M., Karczewski K., Plocinski T., Kurzydowski K.J. Microstructural characterisation of high-entropy alloy  $\text{AlCoCrFeNi}$  fabricated by laser engineered net shaping. *Journal of Alloys and Compounds*, 2015, vol. 648, pp. 751–758. DOI: 10.1016/j.jallcom.2015.05.144.
17. Zhang C., Zhang F., Diao H., Gao M.C., Tang Z., Poplawsky J.D., Liaw P.K. Understanding phase stability of  $\text{Al-Co-Cr-Fe-Ni}$  high entropy alloys. *Materials & Design*, 2016, vol. 109, pp. 425–433. DOI: 10.1016/j.matdes.2016.07.073.



18. Osintsev K.A., Gromov V.E., Konovalov S.V., Panchenko I.A., Vashchuk E.S. Structural-phase state of high-entropy Al-Co-Cr-Fe-Ni alloy obtained by wire-arc additive technology. *Polzunovskiy vestnik*, 2016, no. 1, pp. 141–146. DOI: 10.25712/ASTU.2072-8921.2021.01.020. (In Russian).
19. Zemanate A.M., Júnior A.M.J., Andreani G.F. de Lima, Roche V., Cardoso K.R. Corrosion behavior of AlCoCrFeNi high entropy alloys. *Electrochimica Acta*, 2023, vol. 441, p. 141844. DOI: 10.1016/j.electacta.2023.141844.
20. Niu S., Kou H., Guo T., Zhang Y., Wang J., Li J. Strengthening of nanoprecipitations in an annealed  $\text{Al}_{0.5}\text{CoCrFeNi}$  high entropy alloy. *Materials Science and Engineering: A*, 2016, vol. 671, pp. 82–86. DOI: 10.1016/j.msea.2016.06.040.
21. Ivanov I.V., Emurlaev K.I., Kuper K.E., Safarova D.E., Bataev I.A. Structural transformations during annealing of cold-worked high-entropy alloy  $\text{Al}_{0.3}\text{CoCrFeNi}$ . *Izvestiya vuzov. Chernaya metallurgiya = Izvestiya. Ferrous Metallurgy*, 2022, vol. 65 (8), pp. 539–547. DOI: 10.17073/0368-0797-2022-8-539-547. (In Russian).
22. Zhou J.L., Cheng Y.H., Wan Y.X., Chen H., Wang Y.F., Yang J.Y. Strengthening by Ti, Nb, and Zr doping on microstructure, mechanical, tribological, and corrosion properties of CoCrFeNi high-entropy alloys. *Journal of Alloys and Compounds*, 2024, vol. 984, p. 173819. DOI: 10.1016/j.jallcom.2024.173819.
23. Shi H., Fetzner R., Jianu A., Weisenburger A., Heinzl A., Lang F., Müller G. Influence of alloying elements (Cu, Ti, Nb) on the microstructure and corrosion behaviour of AlCrFeNi-based high entropy alloys exposed to oxygen-containing molten Pb. *Corrosion Science*, 2021, vol. 190, p. 109659. DOI: 10.1016/j.corsci.2021.109659.
24. Pan B., Xu X., Yang J., Zhan H., Feng L., Long Q., Zhou H. Effect of Nb, Ti, and V on wear resistance and electrochemical corrosion resistance of AlCoCrNiMx (M=Nb, Ti, V) high-entropy alloys. *Materials Today Communications*, 2024, vol. 39, p. 109314. DOI: 10.1016/j.mtcomm.2024.109314.
25. Astafurova E.G., Melnikov E.V., Reunova K.A., Moskvina V.A., Astafurov S.V., Panchenko M.Yu., Mikhno A.S., Tumbusova I. Temperature dependence of mechanical properties and plastic flow behavior of cast multicomponent alloys  $\text{Fe}_{20}\text{Cr}_{20}\text{Mn}_{20}\text{Ni}_{20}\text{Co}_{20-x}\text{C}_x$  ( $x = 0, 1, 3, 5$ ). *Fizicheskaya mezhmekhanika = Physical Mesomechanics*, 2021, vol. 24, no. 4, pp. 52–63. DOI: 10.24412/1683-805X-2021-4-52-63. (In Russian).
26. Astafurova E.G., Reunova K.A., Melnikov E.V., Panchenko M.Yu., Astafurov S.V., Maier G.G., Moskvina V.A. On the difference in carbon-and nitrogen-alloying of equiatomic FeMnCrNiCo high-entropy alloy. *Materials Letters*, 2020, vol. 276, p. 128183. DOI: 10.1016/j.matlet.2020.128183.
27. Shubert A.V., Konovalov S.V., Panchenko I.A. A review of research on high-entropy alloys, its properties, methods of creation and application. *Obrabotka metallov (tekhnologiya, oborudovanie, instrumenty) = Metal Working and Material Science*, 2024, vol. 26, no. 4, pp. 153–179. DOI: 10.17212/1994-6309-2024-26.4-153-179.
28. Dalan F.C., Sobrinho A.S.D.S., Nishihara R.K., Santos S.F., Martins G.V., Cardoso K.R. Effect of Nb and Ti additions on microstructure, hardness and wear properties of AlCoCrFeNi high-entropy alloy. *Journal of Alloys and Compounds*, 2025, vol. 1010, p. 177117. DOI: 10.1016/j.jallcom.2024.177117.
29. Ma S.G., Zhang Y. Effect of Nb addition on the microstructure and properties of AlCoCrFeNi high-entropy alloy. *Materials Science and Engineering: A*, 2012, vol. 532, pp. 480–486. DOI: 10.1016/j.msea.2011.10.110.
30. Gromov V.E., Konovalov S.V., Efimov M.O., Panchenko I.A., Shlyarov V.V. Ways to improve the properties of high-entropy alloys Cantor CoCrFeNiMn and CoCrFeNiAl. *Izvestiya vuzov. Chernaya Metallurgiya = Izvestiya. Ferrous Metallurgy*, 2024, vol. 67 (3), pp. 283–292. DOI: 10.17073/0368-0797-2024-3-283-292. (In Russian).
31. Zhang M., Zhang L., Liaw P.K., Li G., Liu R. Effect of Nb content on thermal stability, mechanical and corrosion behaviors of hypoeutectic CoCrFeNiNb<sub>x</sub> high-entropy alloys. *Journal of Materials Research*, 2018, vol. 33 (19), pp. 3276–3286. DOI: 10.1557/jmr.2018.103.
32. Munitz A., Salhov S., Hayun S., Frage N. Heat treatment impacts the micro-structure and mechanical properties of AlCoCrFeNi high entropy alloy. *Journal of Alloys and Compounds*, 2016, vol. 683, pp. 221–230. DOI: 10.1016/j.jallcom.2016.05.034.
33. Güler S., Alkan E.D., Alkan M. Vacuum arc melted and heat treated AlCoCrFeNiTiX based high-entropy alloys: Thermodynamic and microstructural investigations. *Journal of Alloys and Compounds*, 2022, vol. 903, p. 163901. DOI: 10.1016/j.jallcom.2022.163901.
34. Huang S., Wu H., Xu Y., Zhu H. Effects of heat treatment on the precipitation behaviors and mechanical properties of Nb-doped CrMnFeCoNi<sub>0.8</sub> high-entropy alloy. *Materials Science and Engineering: A*, 2023, vol. 885, p. 145611. DOI: 10.1016/j.msea.2023.145611.
35. Fang Y., Ma P., Wei S., Zhang Z., Yang D., Yang H., Konda G.P., Wan S., Jia Y. Selective laser melting of AlCoCrFeMnNi high entropy alloy: Effect of heat treatment. *Journal of Materials Research and Technology*, 2023, vol. 26, pp. 7845–7856. DOI: 10.1016/j.jmrt.2023.09.121.



36. Chen L., Bobzin K., Zhou Z., Zhao L., Öte M., Königstein T., Tan Z., He D. Effect of heat treatment on the phase composition, microstructure and mechanical properties of  $\text{Al}_{0.6}\text{CrFeCoNi}$  and  $\text{Al}_{0.6}\text{CrFeCoNiSi}_{0.3}$  high-entropy alloys. *Metals*, 2018, vol. 8 (11), p. 974. DOI: 10.3390/met8110974.

37. Shang G., Liu Z.Z., Fan J., Lu X.G. Effect of heat treatment on the microstructure and nanoindentation behavior of  $\text{AlCoCrFeNi}$  high entropy alloy. *Intermetallics*, 2024, vol. 169, p. 108302. DOI: 10.1016/j.intermet.2024.108302.

## Conflicts of Interest

The authors declare no conflict of interest.

© 2025 The Authors. Published by Novosibirsk State Technical University. This is an open access article under the CC BY license (<http://creativecommons.org/licenses/by/4.0>).

